Neuroscience 274 (2014) 198–208

RESTING NETWORK IS COMPOSED OF MORE THAN ONE NEURAL PATTERN: AN FMRI STUDY

T.-W. LEE,[a*] G. NORTHOFF[b] AND Y.-T. WU[c]

[a] *Department of Psychiatry, Dajia Lee's General Hospital, Lee's Medical Corporation, Taichung, Taiwan*

[b] *Mind, Brain Imaging and Neuroethics, Institute of Mental Health Research, University of Ottawa, Ottawa, ON K1Z 7K4, Canada*

[c] *Department of Biomedical Imaging and Radiological Sciences, National Yang-Ming University, Taipei, Taiwan*

Abstract—In resting state, the dynamics of blood oxygen level-dependent signals recorded by functional magnetic resonance imaging (fMRI) showed reliable modular structures. To explore the network property, previous research used to construct an adjacency matrix by Pearson's correlation and prune it using stringent statistical threshold. However, traditional analyses may lose useful information at middle to moderate high correlation level. This resting fMRI study adopted full connection as a criterion to partition the adjacency matrix into composite sub-matrices (neural patterns) and investigated the associated community organization and network features. Modular consistency across subjects was assessed using scaled inclusivity index. Our results disclosed two neural patterns with reliable modular structures. Concordant with the results of traditional intervention, community detection analysis showed that neural pattern 1, the sub-matrix at highest correlation level, was composed of sensory–motor, visual associative, default mode/midline, temporal limbic and basal ganglia structures. The neural pattern 2 was situated at middle to moderate high correlation level and comprised two larger modules, possibly associated with mental processing of outer world (such as visuo-associative, auditory and sensory–motor networks) and inner homeostasis (such as default-mode, midline and limbic systems). Graph theoretical analyses further demonstrated that the network feature of neural pattern 1 was more local and segregate, whereas that of neural pattern 2 was more global and integrative. Our results suggest that future resting fMRI research may take the neural pattern at middle to moderate high correlation range into consideration, which has long been ignored in extant literature. The variation of neural pattern 2 could be relevant to individual characteristics of self-regulatory functions, and the disruption in its topology may underlie the pathology of several neuropsychiatric illnesses.

Key words: functional magnetic resonance imaging (fMRI), resting fMRI, functional connectivity, graph theory, community detection, scaled inclusivity.

INTRODUCTION

The human brain is composed of multiple orchestrated networks that support various mental functions. The traditional neuroimaging approach investigating these networks has adopted specific tasks to elicit associated neural responses. In the absence of overt task demands, however, recent studies have demonstrated the existence of spontaneous, low-frequency fluctuations in blood-oxygen level dependent (BOLD) signals of the resting brain that exhibit synchronous patterns across several neural systems, including sensory–motor areas, basal ganglia, visual associative regions, default mode network and so on (Moussa et al., 2012). Functional interaction in the resting brain has been observed not only in the humans but also in other species (Lu et al., 2012).

A network can be represented by vertices (nodes) and links (edges). To elucidate the network property of resting state brain dynamics, there are several options, such as seed-based approach, graph-theoretical model, dynamic causal modeling, Bayes network and so on. Among them, graph theory has recently gained increasing attention in neuroimaging field given its simplicity, less priori (whole-brain analysis in contrast to pre-defined voxels), less assumption (c.f. independent component analysis), capability to derive local and global network properties, and allowance of quantitative assessment of network similarities and differences (Moussa et al., 2012). For graph theory-based approach, it is common to select regions of interest (ROIs) as nodes and construct an adjacency matrix with each cell storing temporal correlation of the correspondent node pair (Jo et al., 2010). The value, correlation coefficient (CC), then serves as an index of functional connectivity strength. After thresholding (TH) to trim up the adjacency matrix, a binary sparse matrix is generated by assigning value 1 to the cells with CCs greater than or equal to TH (edges) and value 0 to the cells with CCs less than TH (no connections). The resultant topology of connectivity pattern provides information about network features, which can be

*Corresponding author. Address: Dajia Lee's General Hospital, Lee's Medical Corporation, Department of Psychiatry No. 2, Bade Street, Dajia District, Taichung City 437, Taiwan ROC. Tel: +886-426862288.

E-mail address: dwlee_ibru@yahoo.com.tw (T.-W. Lee).

Abbreviations: BOLD, blood-oxygen level dependent; CC, correlation coefficient; EPIs, echoplanar images; fMRI, functional magnetic resonance imaging; ROIs, regions of interest; SI, scaled inclusivity; TH, threshold.

http://dx.doi.org/10.1016/j.neuroscience.2014.05.035

derived by several methods, such as graph theoretical approach and fractal model (Olejarczyk, 2007; Rubinov and Sporns, 2010). However, the arbitrary selection of TH may substantially affect small world properties of networks and can be still problematic for ''multiple-threshold-approach'' (Langer et al., 2013).

Dependent on the chosen statistical framework, such as parametric *t*-distribution or non-parametric permutation, the used TH to prune the adjacency matrix can be very harsh, even with only 2% of the strongest connections retained (Schwarz et al., 2008). While the search for the strongest connectivity strengths is certainly statistically robust and well taken, it may nevertheless miss out those connectivity patterns at moderate to high correlation that could be physiologically or neuronally pertinent. The potential relevance of the slightly lower functional connectivity strength is supported by the fact that extraordinary high correlations actually are not that frequently encountered in biological systems that carry out neuropsychological functions (Kriegeskorte et al., 2009; Vul et al., 2009). In addition to the intrinsic differences in the dynamics of different neural substrates, active information integration and neural computation at a particular node may cause change in its waveform and phase delay in its temporal course compared with the signal from adjacent or connected nodes, which may reduce their correlation despite intensive interaction. We therefore argue that current network approach that reserves only the small proportion of edges with highest connectivity strengths may lose useful information that is imperative in the understanding of the whole pictures of the resting brain (Northoff and Bermpohl, 2004; Schneider et al., 2008; Northoff et al., 2011). We assume that at middle to moderate high correlation level there exits other possible partition(s) of network which comprises neural patterns reflecting different perspectives of neuropsychological functions and are also active in resting state. As to the low or insignificant correlation level, we hypothesize that the network partitions contain no modular structures.

Since the brain is efficiently synchronized and intensely interacted so as to cope with the complicated inner and outer challenges in an adoptive and timely manner, it is believed that a particular neural node can reach any other nodes by direct or indirect connections, i.e. full connection. On the other hand, the neural tissue carrying out similar computation is believed to segregate together, which indicates there must be certain kind of modular structures. The above two conditions actually reflect the principles of functional integration and functional segregation (Friston, 2009). The formal definition of full connection is straight forward: for a network, if any selected pair of nodes can reach each other, either directly or indirectly, it is fully connected. Take a network of nodes A–C with direct connections A–B and B–C but not A–C as an example: this network satisfies full connection since A may reach C via B – indirect connection between nodes A and C. This study used full connection as a criterion, instead of traditional arbitrary TH pruning method, to divide the adjacency matrix into several sub-matrices (i.e. decomposed into several network patterns) based on graded connectivity strengths. In addition, the sub-matrices with community number more than 1 were taken as physiologically meaningful partition. Throughout the text, the terms neural/network pattern and sub-matrix were exchangeable, with the former addressing relationship between neural nodes, and the latter emphasizing calculation perspective. Of the decomposed network patterns, we examined the network features and modular structures using graph theory and community detection algorithm (Rubinov and Sporns, 2010; Lancichinetti et al., 2011). The consistency of modular structures for each network was assessed by the indices of scaled inclusivity (SI; Moussa et al., 2012). Our results confirmed the existence of a new partition at middle to moderate high connectivity level which possessed two separate modules and showed good consistency across subjects.

EXPERIMENTAL PROCEDURES

Participants

We recruited 34 healthy subjects with a mean age of 24.7 years (SD = 2.3) and gender balance. All participants were right-handed and were screened to exclude those with a history or evidence of neurological, medical, or psychological disorders, including substance misuse. Before the commencement of experiment, written informed consent approved by the Local Ethics Committee was obtained for each subject. The experimental stimulus was a white central cross subtending at 1.5° of horizontal and vertical visual angle. Each participant was instructed to focus on that cross.

MRI data acquisition and preprocessing

The MRI images were obtained using a 3.0 Tesla scanner (General Electric, Waukesha, WI, USA). A high-resolution spoiled gradient echo (SPGR) structural image and sequential T2*-weighted echoplanar images (EPIs) tracing BOLD dynamics were recorded in resting state. Structural MRI facilitates anatomical description of functional data via registration process (sagittal; TR, 8.1 ms; TE, 3.1 ms; flip angle, 8°; FOV, 250 × 250 mm; matrix, 250 × 250; slice thickness/gap, 1.0/0.0 mm; voxel size, 1 × 1 × 1 mm^3; number of slices, 176). The participants were instructed to focus on a white central cross in the EPI session and a total of 183 functional images were collected for around 6 min with the following parameters: TR, 2.0 s; TE, 30 ms; flip angle, 90°; FOV, 220 × 220 mm; matrix, 96 × 96; slice-thickness/gap, 3.2/0.0 mm; voxel size, 2.3 × 2.3 × 3.2 mm^3; number of slices, 43. The first three EPI volumes were not analyzed to allow for signal equilibrium. The slices for anatomical and functional images both covered the whole brain. Head movement was minimized during scanning using a comfortable external head restraint. We used Analysis of Functional NeuroImages software package (AFNI; http://afni.nimh.nih.gov/afni/) to handle the functional magnetic resonance imaging (fMRI) data. The analytical streamline developed by Jo et al. was adopted to prepare the resting fMRI images (Jo et al., 2010). Preprocessing steps included despike, realignment

(motion corrected), slice-time correction, and spatial normalization to standard stereotaxic space (voxel size $2 \times 2 \times 2$ mm; with respect to the Talairach coordinate system). The resulting movement parameters were checked to ensure that motion did not exceed 1 voxel in any plane. Several regressors were created and modeled as noises, including six movement parameters (pitch, row, yaw, and translation along the *x*-, *y*-, and *z*-directions), third-order polynomials to fit baseline drift, and tissue-based regressors of white matter and ventricles (Jo et al., 2010). After regression, the EPI scans were band passed (0.01–0.1 Hz) and then smoothed (Gaussian kernel with full width at half-maximum set at 6 mm).

Functional connectivity analyses

The prepared fMRI data were segmented into 90 anatomical ROIs according to JuBrain (Eickhoff et al., 2005). Table 1 shows the abbreviations and correspondent numerical codes. The averaged temporal course for each ROI was retrieved and used as a seed vector to correlate with the BOLD dynamics of other ROIs. Pearson's CC was used to represent connectivity strength between two different brain regions. Consequently, a 90 by 90 matrix of CCs was obtained for each participant, also named adjacency matrix. Since CCs generally do not conform to student *t*-distribution, average brain connectivity map was calculated using *z*-transformation (He, 2013). Based on the brain principles of integration and segregation, we used ''full connection'' and ''existence of modular structure'' as two criteria to partition the adjacency matrix into several sub-components, see below.

A network can be denoted by vertices (nodes) and links (edges). It is believed that the human brain is richly interacted and a particular neural node can reach any other nodes by direction or indirect connections. This condition is also called total connection. We used this property to partition the group-averaged adjacency matrix into several sub-matrices (neural pattern) by Tarjan's algorithm (Tarjan, 1972), which starts from an arbitrary node, then visits every node of the graph once by the connected edges. If no nodes are left unreachable in the end, the graph is fully connected. Our analytic processes were composed of 4 steps. First, the CCs of the adjacency matrix were sorted by magnitude. They were used to define consecutive thresholds (THs). Second, TH was selected one at a time, from high to low. The values of the CCs greater than or equal to the TH in the correlation matrix were replaced by ones, otherwise zeroes. The transformed matrix was thus binary in nature. The diagonal ones were disregarded since self-connection was not informative in the calculation. Third, the property of total connectivity was examined for the binary graph. Last, if total connectivity was not met, a lower TH was tested and steps 2–4 were repeated again. If total connectivity was satisfied, the sub-matrix was derived and then, the values of that sub-matrix was set to zero and the steps 2–4 were repeated again for the derivation of next sub-matrix. In summary of the matrix partition strategy, the adjacency matrix is thresholded sequentially by the connectivity strength (i.e. TH) until the surviving network topology meets the criterion of total connection. Tarjan's algorithm was used to fit the principle of ''functional integration'' and Lancichinetti's algorithm was used to meet the principle of ''functional segregation''.

Community detection

A community or module can be described as a cluster of densely interconnected nodes that are sparsely connected with the rest of the network. We explored the

Table 1. Parcellation of 90 brain regions and their abbreviations based on JuBrain atlas (odd number: left; even number: right)

#	Regions	Abbr.	#	Regions	Abbr.
1, 2	Precentral gyrus	PreCG	47, 48	Lingual gyrus	LING
3, 4	Superior frontal gyrus	SFG	49, 50	Superior occipital gyrus	SOG
5, 6	Orbitofrontal cortex (superior)	ORBsup	51, 52	Middle occipital gyrus	MOG
7. 8	Middle frontal gyrus	MFG	53, 54	Inferior occipital gyrus	IOG
9, 10	Orbitofrontal cortex (middle)	ORBmid	55, 56	Fusiform gyrus	FFG
11, 12	Inferior frontal gyrus (opercular)	IFGope	57, 58	Postcentral gyrus	PoCG
13, 14	Inferior frontal gyrus (triangular)	IFGtri	59, 60	Superior parietal lobule	SPL
15, 16	Inferior frontal gyrus (orbital)	IFGori	61, 62	Inferior parietal lobule	IPL
17, 18	Rolandic operculum	ROL	63, 64	Supramarginal gyrus	SMG
19, 20	Supplementary motor area	SMA	65, 66	Angular gyrus	ANG
21, 22	Olfactory cortex	OLF	67, 68	Precuneus	PCUN
23, 24	Superior frontal gyrus (medial)	SFGmed	69, 70	Paracentral lobule	PCL
25, 26	Obitofrontal gyrus (medial)	ORBmed	71, 72	Caudate	CAU
27, 28	Rectus gyrus	REC	73, 74	Putamen	PUT
29, 30	Insula	INS	75, 76	Pallidum	PAL
31, 32	Anterior cingulate gyrus	ACG	77, 78	Thalamus	THA
33, 34	Middle cingulate gyrus	MCG	79, 80	Heschl gyrus	HES
35, 36	Posterior cingulate gyrus	PCG	81, 82	Superior temporal gyrus	STG
37, 38	Hippocampus	HP	83, 84	Temporal pole	TPO
39, 40	Parahippocampal gyrus	PHG	85, 86	Middle temporal gyrus	MTG
41, 42	Amygdala	AMY	87, 88	Temporal pole (medial)	TPOmed
43, 44	Calcarine cortex	CAL	89, 90	Inferior temporal gyrus	ITG
45, 46	Cuneus	CUN			

community structures for each of the sub-matrices or network patterns by the algorithm Order Statistics Local Optimization Method (OSLOM, 2nd version; http://www.oslom.org/). OSLOM2 is based on a local fitness function that optimizes the statistical significance of a sub-graph compared with the random fluctuation of a global null model (Lancichinetti et al., 2011), with the performance comparable to the best existing algorithms in several artificial benchmark networks (Good et al., 2010; Bassett et al., 2011). We applied OSLOM2 to the sub-matrices of group-level adjacency matrix as well as to those of the individual-level analyses for a checkup of modular consistency (see the section of *Scaled inclusivity* below). Only the neural pattern equipped with more than 1 module was viewed as valid partition and was imported into further analyses.

Scaled inclusivity analysis for modular consistency

Although it is generally accepted to take mean/average as a representative of the individuals, it is important to test whether our new strategy of network partition, especially at middle to moderate high correlation strength, is reliable. For each valid partition of adjacency matrix (neural pattern), we compared the modular structures at group level with those at individual level using the algorithm of SI which has been successfully applied in complex network and resting fMRI connectome data (Steen et al., 2011; Moussa et al., 2012). The principle is straightforward; for any two modules in two networks, say module x in network A and module y in network B, a consistency index (CI) can be calculated by the formula $CI = |Ax \bigcap By|/|Ax| * |Ax \bigcap By|/|By|$, where $|\blacktriangledown|$ means the size/cardinality of a set. Next, a consistency vector is generated by assigning the intersected nodes ($|Ax \bigcap By|$) as ones and the remaining nodes as zeroes and then weighted by CI. For every possible module combination from neural pattern A (e.g. group-level) and B (e.g. individual-level), such as AxBx, AxBz, AyBx, AyBz and so on, there is a correspondent consistency vector. Sum them up would yield the SI indices for each node and constitute an SI vector. In this study, regarding a particular neural pattern, the SI vector for each subject was calculated and then averaged, with the group-level result served as a template.

To provide statistical inference, we performed a simulation of 10,000 times for each network pattern as follows. First, we retained the number and size of modules for each subject so that the global modular organization was unchanged but the contents of modules were left unassigned. Second, we filled in the empty modules in the sub-matrix with randomly selected neural nodes. Last, we computed the SI indices/vector as above, also taking group-level modularization as a reference. The statistics of consistency can then be inferred from the distribution of the simulation results of SI indices/vector. Note that in previous literature, CI is also named SI and we differentiated them to avoid ambiguity. In the text, SI indices and CI indices refer to the end results and the intermediate results of the SI calculation, respectively.

Graph theoretical analysis

We applied graph theory and Brain Connectivity Toolbox (http://www.brain-connectivity-toolbox.net) to examine the differences in different network patterns defined by correlation strength, total connection and existence of modular structure, as described above. The indicators of network integration, segregation, nodal centrality, and modularity were compared by paired *t*-tests, including characteristic path length, global efficiency, clustering coefficient, transitivity, local efficiency, betweenness centrality, and Newman's modularity (Leicht and Newman, 2008). The formal mathematical definition of the above network measures is described in detail elsewhere (Rubinov and Sporns, 2010).

RESULTS

Fig. 1 illustrates the group-averaged functional connectivity across 90 ROIs. By graded connectivity strengths and total connection criterion, the group-level adjacency matrix can be partitioned into eight sub-matrices, see Fig. 2. Our main analyses started from here.

Modular analyses

At group level, OSLOM2 detected five and two modules in sub-matrices 1 and 2, respectively. For the remaining sub-matrices, the module numbers were zeroes. At individual level, the averaged numbers of modules of the first two sub-matrices by the order of connectivity strengths were 4.42 and 2.00. Other details are summarized in Table 2. Given the modularity results, subsequent analyses focused only on the two sub-matrices with higher functional connectivity strength.

For sub-matrix 1, the noticed five modules were visual associative areas (43, 44, 45, 46, 47, 48, 49, 50, 51, 52, 53, 54, 55, 56, 89, 90), basal ganglia (71, 72, 73, 74, 75, 76), sensory–motor and acoustic regions (1, 2, 11, 12, 17, 18, 19, 20, 29, 30, 57, 58, 59, 60, 61, 62, 63, 64, 69, 70, 79, 80, 81, 82), temporal limbic regions (37, 38, 39, 40, 41, 42), and default mode and midline structures (3, 4, 5, 6, 7, 8, 9, 10, 13, 14, 15, 16, 23, 24, 25, 26, 27, 28, 31, 32, 33, 34, 35, 36, 65, 66, 67, 68, 85, 86, 87, 88). The numbers in the parentheses are area codes, please refer to Table 1. The five modules in group-averaged sub-matrix 1 are color-coded and illustrated in Fig. 3. Our results of the five modules were concordant with previous fMRI studies which investigated the network of highest connectivity strengths (after stringent statistical thresholding) in the resting brain (Moussa et al., 2012), indicating that the neural pattern 1 based on full connection criteria was compatible with the traditional approach which trimmed adjacency matrix using stringent thresholds, and also suggesting that the findings of neural pattern 2 would be novel, see below.

The sub-matrix 2 was constituted by two modules, one comprising sensory–motor, acoustic and visual associated regions (1, 2, 11, 12, 17, 18, 19, 20, 29, 30, 33, 34, 43, 44, 45, 46, 47, 48, 49, 50, 51, 52, 53, 54, 55, 56, 57, 58, 59, 60, 63, 64, 69, 70, 79, 80, 81, 82,

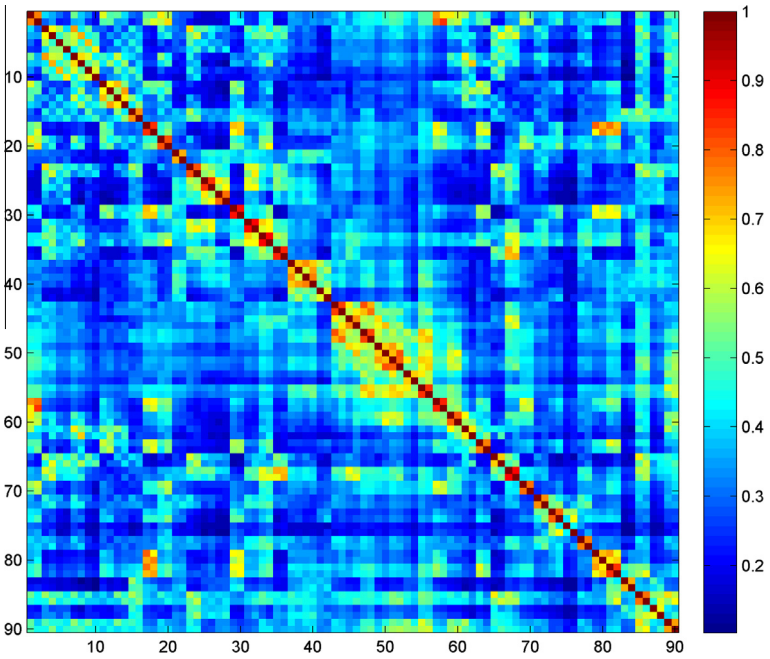

Fig. 1. The correlation matrix is 90 × 90 and has values ranging from 0 to 1, constructed by BOLD temporal courses of 90 ROIs. The numbers at abscissa and ordinate are the area codes (see Table 1). The color bar is located at the right-hand side. (For interpretation of the references to color in this figure legend, the reader is referred to the web version of this article.)

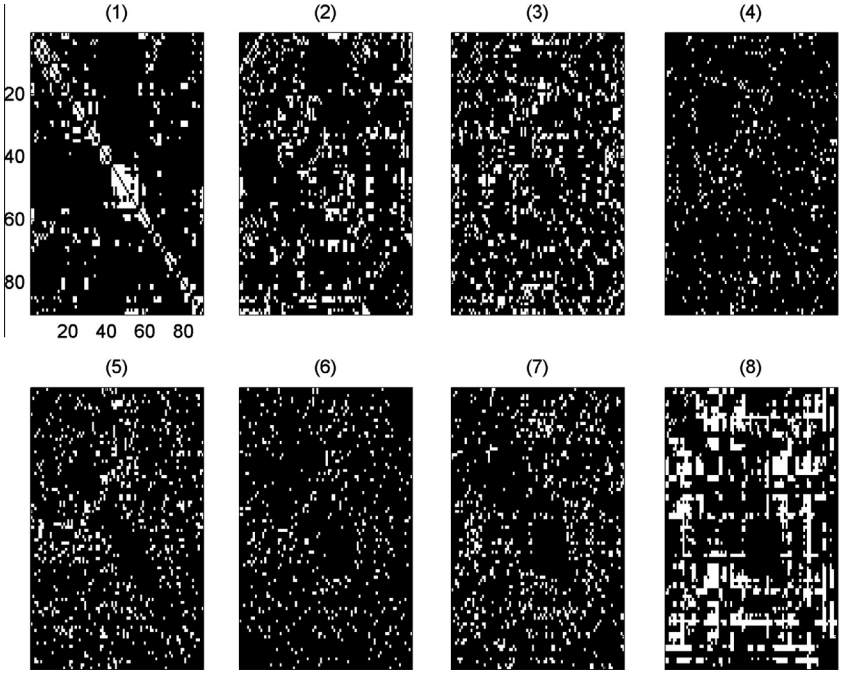

Fig. 2. The group-averaged adjacency matrix was decomposed into eight sub-matrices (neural patterns). The subplots (1) to (8) are arranged by correlation strengths, from high to low. The numbers at abscissa and ordinate are the area codes (see Table 1).

85, 86), and the other comprising temporal limbic, midline and default-mode networks (3, 4, 5, 6, 7, 8, 9, 10, 13, 14, 15, 16, 21, 22, 23, 24, 25, 26, 27, 28, 31, 32, 35, 36, 37, 38, 39, 40, 41, 42, 43, 44, 47, 48, 61, 62, 65, 66, 67, 68, 71, 72, 77, 78, 83, 84, 85, 86, 87, 88, 89, 90), see Fig. 4. They were partly overlapped at calcarine, lingual and middle temporal cortices (43, 44, 47, 48, 85, 86). It is noteworthy that the modules of sub-matrix 2 were not simply the confluent of modular structures of sub-matrix 1 since the two sub-matrices were non-overlapping. Sub-matrices 1 and 2 had distinct network topology and features, see next section for detail.

The modular consistency of group-level versus individual-level networks was assessed by SI and

Table 2. The details of adjacency matrix partition

Sub-matrices	1	2	3	4	5	6	7	8
Group level								
Module No.	5	2	0	0	0	0	0	0
Max CC	0.789	0.520	0.425	0.363	0.345	0.314	0.295	0.261
Min CC	0.520	0.425	0.363	0.345	0.314	0.295	0.261	0.103
Individual level								
Module No.	4.42	2.00	0.00	0.29	0.06	0.03	0.11	0.03
(SD)	1.44	0.55	0.00	0.70	0.23	0.17	0.32	0.17

CC: correlation coefficient; SD: standard deviation.

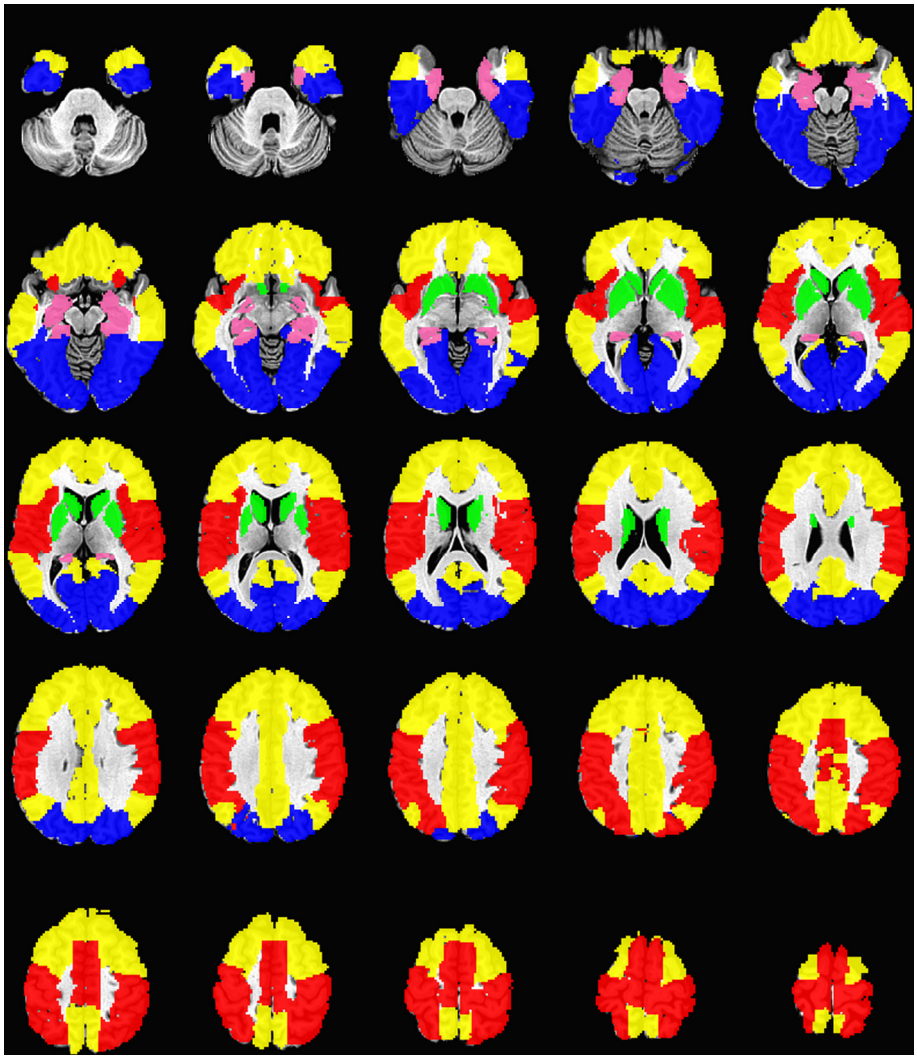

Fig. 3. The summary of modular structure in neural pattern 1, i.e. the sub-matrix with highest connectivity strength. Blue: visual associative areas; red: sensory–motor regions; green: basal ganglia, pink: temporal limbic regions; yellow: midline and default mode structures. The five modules were superimposed on a T1 structural template in axial section from $z = -31$ mm to $z = 65$ mm with an inter-slice gap of 4 mm ($z = 0$ at the plane bridging anterior and poster commissure). (For interpretation of the references to color in this figure legend, the reader is referred to the web version of this article.)

random permutation for 10,000 times. The results were quite robust with the SI values of most neural nodes in sub-matrices 1 and 2 less than p value 0.05/90 after Bonferroni correction. Our results implied that the modular organization disclosed in the group-level analysis also existed at individual level. The results of SI analyses and random permutation for each node are highlighted in Fig. 5.

Comparison of network features

The differences in network features of sub-matrices 1 and 2, such as characteristic path length, global efficiency,

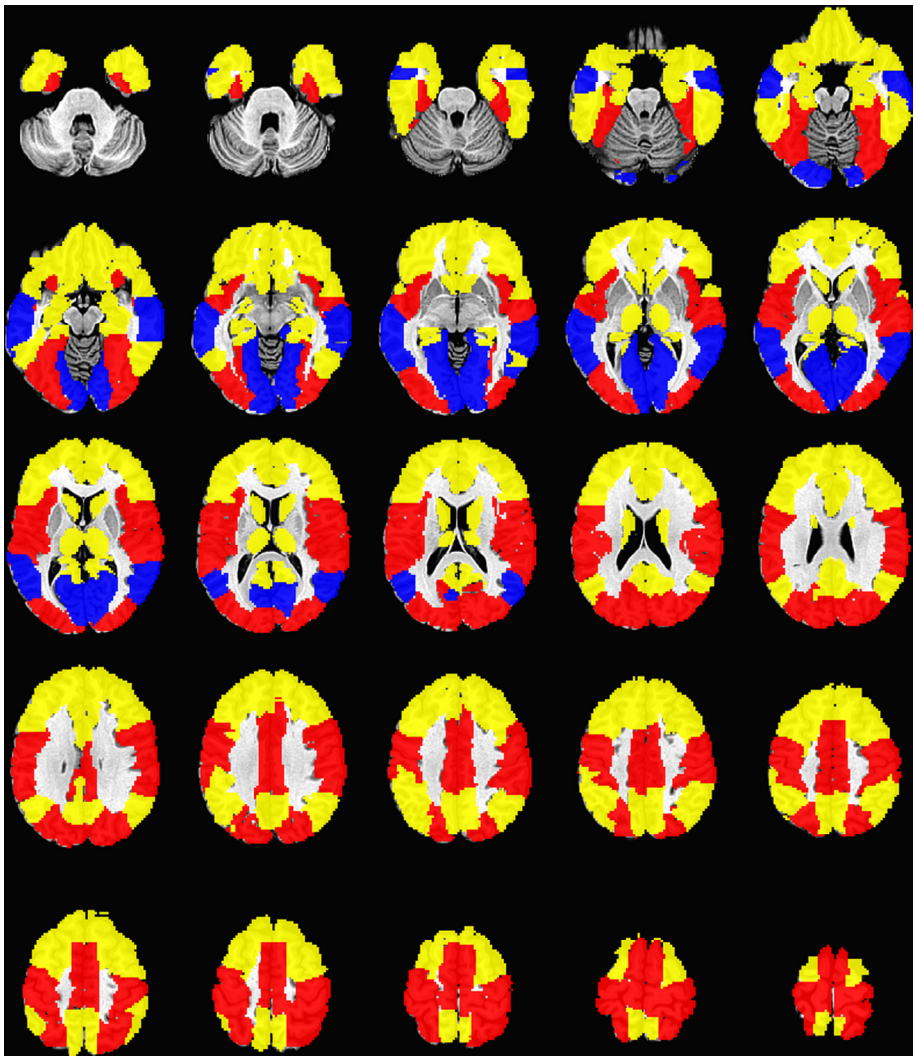

Fig. 4. The summary of modular structure in neural pattern 2, i.e. the sub-matrix with 2nd highest connectivity strength. The two modules were color-coded in yellow and red, and their overlapped regions were indicated by blue color. The two modules were superimposed on a T1 structural template in axial section from $z = -31$ mm to $z = 65$ mm with an inter-slice gap of 4 mm ($z = 0$ at the plane bridging anterior and poster commissure). (For interpretation of the references to color in this figure legend, the reader is referred to the web version of this article.)

clustering coefficient, transitivity, local efficiency, and Newman's modularity for each participant, were calculated by graph theory and examined by paired *t*-tests. Compared with sub-matrix 2, sub-matrix 1 had longer characteristic path length, lower global efficiency, and higher clustering coefficient, transitivity, local efficiency and modularity. The statistics were generally at the level of 10^{-20}, summarized in Table 3.

Betweenness centrality is a local index counting the number of shortest paths from all pairs of vertices passing through a particular node, which can be viewed as an indicator of "hub" (Tomasi and Volkow, 2011). Direct comparison of sub-matrices 1 and 2 revealed several regions showing significant differences in the nodal centrality, including right PreCG (2), left MFG (7), left ROL (17), left SFGmed (23), right ORBmed (26), right STG (82) and left MTG (85). The numbers in the parenthesis are area codes. The significant results of betweenness centrality are summarized in Table 3.

DISCUSSION

It is well established that the resting brain possesses intrinsic dynamics and interacting structures. Previous fMRI research has explored the correlation of BOLD signals in resting state and has used harsh threshold to reveal the neural interaction patterns (Moussa et al., 2012). However, massive information exchange, integration and computation could make the connectivity strengths of a network situated at middle to moderate high correlation range, due to resultant change in waveform and phase delay. Traditional approach thus may disregard this important feature. To address the pitfall, graded connectivity and total connection were combined to partition the adjacency/correlation matrix of BOLD signals from 90 ROIs into separate components. Only the sub-matrices showing reliable modular structures were taken as meaningful partitions. These two terms were applied to realize the principles of functional integration and

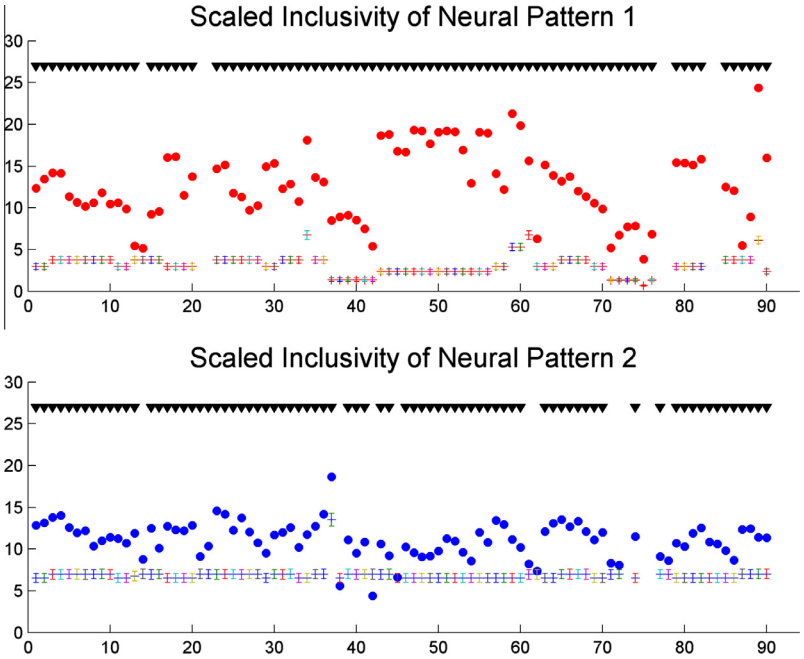

Fig. 5. Comparison of modular consistency in sub-matrices 1 (upper subplot) and 2 (lower subplot) with the results of random permutation of modular content for 10,000 times. The values of scaled inclusivity and the 90 coded areas are indicated at abscissa and ordinate, respectively. Filled circles are the data points and crosses are the means of simulated SIs (±1SD). Black triangles pointing down symbolize the comparisons that showed significant statistical differences, less than a corrected p value of 0.00056 (0.05/90).

Table 3. The comparison of graph features of sub-matrices 1 and 2

	Sub-matrix 1 mean (SD)	Sub-matrix 2 mean (SD)	Mean diff (SD)	t-Value	p-Value
Charp	2.85 (0.18)	2.15 (0.06)	0.70 (0.18)	22.76	10^{-21}
Eglob	0.38 (0.04)	0.50 (0.02)	−0.12 (0.03)	−25.08	10^{-23}
Clust	0.49 (0.04)	0.24 (0.02)	0.25 (0.04)	37.97	10^{-29}
Transitivity	0.51 (0.06)	0.24 (0.02)	0.27 (0.05)	32.52	10^{-26}
Eloc	0.62 (0.04)	0.45 (0.02)	0.17 (0.05)	20.83	10^{-20}
Modularity	0.47 (0.06)	0.28 (0.03)	0.19 (0.05)	23.45	10^{-22}
Betweenness centrality					
PreCG (R)	189.55 (163.38)	89.10 (89.86)	100.45 (157.22)	3.73	0.00073*
MFG (L)	303.44 (231.02)	129.92 (129.83)	173.52 (210.48)	4.81	0.000033
ROL (L)	190.56 (173.72)	72.39 (63.95)	118.17 (171.18)	4.03	0.00031
SFGmed (L)	228.71 (144.54)	130.94 (120.39)	97.77 (134.82)	4.23	0.00018
ORBmed (R)	140.22 (111.90)	47.17 (32.36)	93.05 (110.04)	4.93	0.000023
STG (R)	326.43 (285.71)	156.14 (133.46)	170.29 (232.01)	4.28	0.00015
MTG (L)	535.48 (408.41)	268.12 (164.73)	267.36 (413.71)	3.77	0.00065*

Charp, characteristic path length; Eglob: global efficiency; Clust, clustering coefficient; Eloc, local efficiency.
Threshold of p-value was set at 0.05/90 = 0.00056.
* Indicates approaching significance; d.f. = 33.

segregation. The analytic results were grossly concordant with our expectation. In addition to the frequently reported community structures at strongest correlation range, there was another network next to it at a slightly lower correlation level, constituted by two larger communities and equipped with good consistency across subjects.

Modular structures of resting network

To facilitate the comparison with previous literature (He et al., 2009; Moussa et al., 2012), we parcellated the brain into 90 ROIs and binarized the adjacency matrix. With the similar pre-processing steps, we may infer whether the derived modules of different neural patterns may correspond to the results of previous studies or are novel discovery. According to the full connection criterion, it was revealed that the correlation matrix of BOLD dynamics can be decomposed into eight sub-matrices, from high-degree to low-degree correlation. Only the first two sub-matrices (neural patterns) demonstrated reliable modular structures. The characteristics of the remaining six sub-matrices were thus not scrutinized. The modular organization of the first neural pattern nicely coincided with previous reports that usually comprise sensory–motor regions, visual associative areas, default-mode network and basal ganglia (Moussa et al., 2012). The second

neural pattern was composed of two larger communities. One was responsible for processing and manipulation of external world, including sensory–motor, acoustic and visual-associated regions. The other was relevant to inner state homeostasis and self-related functions, such as temporal limbic, midline and default-mode structures (Northoff and Bermpohl, 2004). It is important to note that the two communities detected in sub-matrix 2 were not simply equal to the union of the communities in sub-matrix 1. The sub-matrices 1 and 2 were non-overlapping and were distinctive in their topology. Their differences were computed by graph theoretical approach and paired *t*-tests, discussed in next section.

It is acknowledged that the metabolic and circulatory changes associated with the BOLD signal are driven by the bioelectrical and biochemical reactions at the neuronal dendrites (Logothetis et al., 2001). The fact that the global metabolic rate in resting state is similar to that in carrying out psychological tasks implies significant functioning associated with the resting brain (Sokoloff et al., 1955; Gusnard and Raichle, 2001). ''Resting'' thus does not necessarily mean ''idling''. From neurobiological perspective, continuous neurotransmission and intracellular molecular cascade may partly explain the energy consumption. From neuropsychological perspective, resting state is relevant to self-functioning (Northoff and Bermpohl, 2004) and consolidation of learning or memory (Frey et al., 1996). Regionally, the metabolic rate in resting state does not attenuate or even increases in default-mode and midline systems (Gusnard and Raichle, 2001; Northoff and Bermpohl, 2004). Temporal limbic structures also seem to keep higher metabolic rate in resting state (Shin et al., 2011; Shen et al., 2012). Together, the two modules in neural pattern 2 may respectively show lower and higher metabolic rate in resting state which respond to the challenges of external world and homeostasis requirement of inner state.

The above analysis was based on the averaged functional connectivity. We also applied similar analytic process to each participant. To examine whether the group results also appeared at the individual level, SI index was adopted to examine the modular consistency (Steen et al., 2011; Moussa et al., 2012). Our analyses verified that the structures of five modules in sub-matrix 1 ($r = 0.789–0.520$) and two modules in sub-matrix 2 ($r = 0.520–0.425$) were quite robust. In accord, the mean module numbers in sub-matrices 1 and 2 were 4.42 and 2.00, respectively. Together with the group results and the cross-subject structural stability, our conjecture of extra network(s) at different correlation range is confirmed. The negative modular finding for the sub-matrices at low correlation end is reasonable.

Comparison of network features of neural patterns 1 and 2

Vertices (nodes) and links (edges) describe a network. Network features can be largely categorized into either local or global and may target the topological aspects of segregation or integration. Since the neural patterns 1 and 2 were non-overlapping, it is not surprising that all their graph indices were different significantly. Graph theory uses the shortest path length between two nodes to suggest functional integration, with the shorter path implying stronger potential for integration. The characteristic path length is defined as the averaged shortest path lengths between all pairs of vertices in a network, whereas global efficiency is the averaged inverse shortest path length. Both indicators probe the integrative aspect of a network, but they differ in their relative bias by longer or shorter paths. Take an extreme case as example, a disconnected graph may have an infinite characteristic path length but limited global efficiency because the inverse of infinite path length is zero. Simultaneous inspection of the two indices is thus not redundant. Despite lower correlation ranking, neural pattern 2 showed stronger integration property than that of neural pattern 1. The finding indicated that neural pattern 2 was more ''interactive'' than neural pattern 1.

Neural tissues executing similar functions tend to aggregate together. Segregation measures such as clustering coefficient and transitivity are based on the calculation of triangles per node, with a high number of triangles indicating segregation. The rationale to use triangles as topological mediates of segregation is that the neighbors of a triangle's vertex are also each other's neighbors, as opposed to three linked vertices that do not form a triangle. The fraction of triangles out of all ''possible'' triangles (i.e., any selected two edges from a vertex) for a particular neural node constitutes the nodal clustering index. Transitivity is a collective measure derived from all triangles out of all possible triangles in a network without going through the clustering index for each individual node, which is less biased by the low-degree vertex (low degree means less connections). Local efficiency of a ''network'' is a different segregation measure, which is the average local efficiency of ''nodes.'' Instead of counting triangles, local efficiency is defined by the shortest path length, topology and connectivity of its neighbors. Specifically, for a particular node A and any other two nodes B and C linked to A, the inverse of the shortest path length between B and C passing A's neighbor is calculated. The calculation is then extended to all neighboring node pairs of A, summed up, and then normalized by the number of all possible combinations. For all the segregation indices, in opposition to the integration counterparts, neural pattern 1 was higher than neural pattern 2. Neural pattern 1 possessed stronger modular structures and also had higher modularity index.

Put the graph theoretical results together, we inferred that neural pattern 1 (and traditional resting network approach) was characterized by local segregation property, while neural pattern 2 reflected the global integration dimension. It is noteworthy that the conditions of moderate high correlation and lower modularity degree do not necessarily occur together. Further, if the community revealed in neural pattern 2 was just the reminiscent of neural pattern 1 but removing connections with highest correlations, the modular structures would be grossly preserved. We thus

regard our findings heuristic. The inference was also compatible with our assumption that intense information exchange, integration and computation should make the correlation between neural nodes weaker, i.e. the lower connectivity strengths in neural pattern 2.

Betweenness centrality is another local quantity, defined as the fraction of all shortest paths in the network passing through an individual node. The nodes with higher betweenness centrality can play a role in bridging disparate parts of a network. PreCG, MFG, ROL, SFGmed, ORBmed, STG and MTG were the neural nodes showing stronger ''hub'' property in neural pattern 1 compared with those in neural pattern 2. Since neural pattern 1 was more segregated or localized, these nodes may carry the ''integrating'' function to facilitate the cross-talks between different modules. Concordant with the ''hub'' property inferred from our analyses, five out of the seven neural nodes were situated in the frontal lobe, where diverse/cross-modal information is processed, action is evaluated and planned, and higher cognitive functions are endorsed, such as executive control, cognition–emotion regulation, sensory–motor integration, action planning, knowledge of other person and so on (Goldman-Rakic, 1996; Gray et al., 2002; Mitchell et al., 2002). The orbitofrontal cortex receives input from all the sensory modalities and ORBmed has direct projection from the hippocampus (Ongur and Price, 2000; Kringelbach and Rolls, 2004), which are further conveyed to visceromotor structures to regulate the inner state. Superior temporal gyrus is not only a multi-modal interface where dorsal and ventral visual inputs converge, it also involves in the processing of species-specific vocalizations, and linguistic and social information (Karnath, 2001).

It is noteworthy that earlier papers (Fransson, 2005), have assumed that the brain toggles between an introspectively oriented mode and an extrospectively oriented mode. This insightful argument and/or assumption cannot get support from traditional graph analysis since they generally produce ''local'' modules – that is what we found in neural pattern 1. Our findings of neural pattern 2 provide empirical evidence that the brain is indeed organized in some way that underlies the introspective and extrospective switch.

CONCLUSION, LIMITATION AND FUTURE DIRECTION

This resting fMRI study explored the network structures and the associated features based on the correlation matrix of BOLD dynamics across 90 pre-defined ROIs. Unlike harsh thresholding in previous research, we partitioned the network consecutively based on the property of full connection and graded connectivity strengths, and studied their characteristics. The condition of existence of community structures was used to constrain valid partition. In addition to the frequently reported network surviving stringent connectivity strength (neural pattern 1), we unveiled a network that has long been ignored and was situated at middle to moderate high correlation range (neural pattern 2). The property of neural pattern 1 was more local and congregative whereas that of the neural pattern 2 was more global and integrative. Let us use mountain-plate analogy to make the distinction clearer. At above-sea level 2000 m, several independent mountains demonstrated prominent modular structures. However, deeper inspection will reveal that there are actually two collided/interacted tectonic plates (neural pattern 2) underlying the mountains (neural pattern 1).

The implication of the neural pattern at middle high correlation level in neuropsychiatry would be very interesting. It is acknowledged that one of the core pathologies in major neuropsychiatric diseases is disconnection or connectivity change, and the neural pattern 2 was more relevant to the integrating dimension of resting brain network. We expected disrupted topology at this level in several mental illnesses, such as schizophrenia or affective disorders. The variation in topology and weights of the neural pattern at middle high correlation range may also correspond with individual styles in self-regulatory functions. We suggest future resting fMRI studies incorporate this partition into consideration instead of just casting it off. Although full connection is a reasonable constraint, this work resorted to disjoint decomposition to derive composite submatrices. It is possible that the partition allowing partial overlaps or non-overlapping gaps may yield neural pattern 3 and more. Variation in the preparatory processes, like different ROI parcellation scheme and calculation of weighted matrix without binarization, may also influence the results. Further, it is worthwhile to construct multi-layer network to investigate how networks with different connectivity strengths interact with each other and study all the neural patterns as a whole.

Acknowledgement—This work was supported by Hangzhou Normal University, China.

REFERENCES

Bassett DS, Wymbs NF, Porter MA, Mucha PJ, Carlson JM, Grafton ST (2011) Dynamic reconfiguration of human brain networks during learning. Proc Natl Acad Sci U S A 108:7641–7646.

Eickhoff SB, Stephan KE, Mohlberg H, Grefkes C, Fink GR, Amunts K, Zilles K (2005) A new SPM toolbox for combining probabilistic cytoarchitectonic maps and functional imaging data. Neuroimage 25:1325–1335.

Fransson P (2005) Spontaneous low-frequency BOLD signal fluctuations: an fMRI investigation of the resting-state default mode of brain function hypothesis. Hum Brain Mapp 26:15–29.

Frey U, Frey S, Schollmeier F, Krug M (1996) Influence of actinomycin D, a RNA synthesis inhibitor, on long-term potentiation in rat hippocampal neurons in vivo and in vitro. J Physiol 490(Pt 3):703–711.

Friston KJ (2009) Modalities, modes, and models in functional neuroimaging. Science 326:399–403.

Goldman-Rakic PS (1996) The prefrontal landscape: implications of functional architecture for understanding human mentation and the central executive. Philos Trans R Soc Lond B Biol Sci 351:1445–1453.

Good BH, de Montjoye YA, Clauset A (2010) Performance of modularity maximization in practical contexts. Phys Rev E 81:046106.

Gray JR, Braver TS, Raichle ME (2002) Integration of emotion and cognition in the lateral prefrontal cortex. Proc Natl Acad Sci U S A 99:4115–4120.
Gusnard DA, Raichle ME (2001) Searching for a baseline: functional imaging and the resting human brain. Nat Rev Neurosci 2:685–694.
He BJ (2013) Spontaneous and task-evoked brain activity negatively interact. J Neurosci 33:4672–4682.
He Y, Wang J, Wang L, Chen ZJ, Yan C, Yang H, Tang H, Zhu C, Gong Q, Zang Y, Evans AC (2009) Uncovering intrinsic modular organization of spontaneous brain activity in humans. PLoS ONE 4:e5226.
Jo HJ, Saad ZS, Simmons WK, Milbury LA, Cox RW (2010) Mapping sources of correlation in resting state FMRI, with artifact detection and removal. Neuroimage 52:571–582.
Karnath HO (2001) New insights into the functions of the superior temporal cortex. Nat Rev Neurosci 2:568–576.
Kriegeskorte N, Simmons WK, Bellgowan PS, Baker CI (2009) Circular analysis in systems neuroscience: the dangers of double dipping. Nat Neurosci 12:535–540.
Kringelbach ML, Rolls ET (2004) The functional neuroanatomy of the human orbitofrontal cortex: evidence from neuroimaging and neuropsychology. Prog Neurobiol 72:341–372.
Lancichinetti A, Radicchi F, Ramasco JJ, Fortunato S (2011) Finding statistically significant communities in networks. PLoS ONE 6:e18961.
Langer N, Pedroni A, Jancke L (2013) The problem of thresholding in small-world network analysis. PLoS ONE 8:e53199.
Leicht EA, Newman ME (2008) Community structure in directed networks. Phys Rev Lett 100:118703.
Logothetis NK, Pauls J, Augath M, Trinath T, Oeltermann A (2001) Neurophysiological investigation of the basis of the fMRI signal. Nature 412:150–157.
Lu H, Zou Q, Gu H, Raichle ME, Stein EA, Yang Y (2012) Rat brains also have a default mode network. Proc Natl Acad Sci U S A 109:3979–3984.
Mitchell JP, Heatherton TF, Macrae CN (2002) Distinct neural systems subserve person and object knowledge. Proc Natl Acad Sci U S A 99:15238–15243.
Moussa MN, Steen MR, Laurienti PJ, Hayasaka S (2012) Consistency of network modules in resting-state FMRI connectome data. PLoS ONE 7:e44428.
Northoff G, Bermpohl F (2004) Cortical midline structures and the self. Trends Cogn Sci 8:102–107.
Northoff G, Qin P, Feinberg TE (2011) Brain imaging of the self–conceptual, anatomical and methodological issues. Conscious Cogn 20:52–63.
Olejarczyk E (2007) Application of fractal dimension method of functional MRI time-series to limbic dysregulation in anxiety study. Conf Proc IEEE Eng Med Biol Soc 2007:3408–3410.
Ongur D, Price JL (2000) The organization of networks within the orbital and medial prefrontal cortex of rats, monkeys and humans. Cereb Cortex 10:206–219.
Rubinov M, Sporns O (2010) Complex network measures of brain connectivity: uses and interpretations. Neuroimage 52: 1059–1069.
Schneider F, Bermpohl F, Heinzel A, Rotte M, Walter M, Tempelmann C, Wiebking C, Dobrowolny H, Heinze HJ, Northoff G (2008) The resting brain and our self: self-relatedness modulates resting state neural activity in cortical midline structures. Neuroscience 157:120–131.
Schwarz AJ, Gozzi A, Bifone A (2008) Community structure and modularity in networks of correlated brain activity. Magn Reson Imaging 26:914–920.
Shen X, Liu H, Hu Z, Hu H, Shi P (2012) The relationship between cerebral glucose metabolism and age: report of a large brain PET data set. PLoS ONE 7:e51517.
Shin J, Tsui W, Li Y, Lee SY, Kim SJ, Cho SJ, Kim YB, de Leon MJ (2011) Resting-state glucose metabolism level is associated with the regional pattern of amyloid pathology in Alzheimer's disease. Int J Alzheimer Dis 2011:759780.
Sokoloff L, Mangold R, Wechsler RL, Kenney C, Kety SS (1955) The effect of mental arithmetic on cerebral circulation and metabolism. J Clin Invest 34:1101–1108.
Steen M, Hayasaka S, Joyce K, Laurienti P (2011) Assessing the consistency of community structure in complex networks. Phys Rev E 84:016111.
Tarjan R (1972) Depth-first search and linear graph algorithms. SIAM J Comput 1:146–160.
Tomasi D, Volkow ND (2011) Functional connectivity hubs in the human brain. Neuroimage 57:908–917.
Vul E, Harris C, Winkielman P, Pashler H (2009) Puzzlingly high correlations in fMRI studies of emotion, personality, and social cognition. Perspect Psychol Sci 4:274–290.

(Accepted 16 May 2014)
(Available online 29 May 2014)